nature chemistry

ARTICLES

https://doi.org/10.1038/s41557-021-00750-x

Check for updates

Organocatalyst-controlled site-selective arene C–H functionalization

Jian-Hui Mao[1,4], Yong-Bin Wang[1,4] ✉, Limin Yang[2,4], Shao-Hua Xiang[3], Quan-Hao Wu[1], Yuan Cui[1], Qian Lu[1], Jie Lv[1], Shaoyu Li[3] and Bin Tan[1] ✉

Over the past three decades, organocatalysis has emerged as a powerful catalysis platform and has gradually been incorporated into the routine synthetic toolbox to obtain chiral molecules. However, its application in the site- and enantioselective functionalization of inactive aryl C–H bonds remains in its infancy. Here, we present an organocatalyst-controlled *para*-selective arene C–H functionalization strategy that addresses this issue, which remains an enduring challenge in arene functionalization chemistry. By emulating enzyme catalysis, the chiral phosphoric acid catalyst offers an ideal chiral environment for stereoinduction, and the projecting substituents give control of chemo- and site-selectivity. Various types of nucleophile are compatible with this method, affording more than 100 *para*-selective adducts with stereodefined carbon centres or axes in viable molecular contexts. This protocol is expected to provide a general strategy for *para*-selective functionalization of arene C–H bonds in a controlled manner.

Direct site- and enantioselective arene C–H functionalization streamlines methods for acquiring multi-substituted chiral arene structures[1–3]. Among the latent reactive sites on a substituted benzene ring, functionalization of the most distal *para*-C–H bond appears particularly challenging due to its relative remoteness from the directing handle. By virtue of the innate substituent orientation effect enforced by electron-donating arene substituents, such transformations could be enabled by S_EAr-type reactions[4,5] and C–H substitution via a radical path[6–8]. However, rival *ortho*-C–H bond functionalization presents in most scenarios. A chelation-assisted C–H activation strategy could override the inherent electronic bias by regulating site-selectivity through coordination with the metal centre; however, only limited examples of D-shaped assemblies—formed by the substrate, directing group and transition metal—are currently available[9–17], so strategies for ideal *para*-selective reactions remain to be developed (Fig. 1a). Accordingly, a robust protocol for functionalizing the arene C–H bond with competent *para* control is still a challenging issue in conventional arene chemistry. More importantly, the harsh reaction conditions needed to overcome the high dearomatization barrier and/or to provoke inert C–H bond activation/insertion could hinder achieving the desired site- and enantiocontrol. On a related note, a more efficient catalyst-controlled strategy is realized in nature by enzymatic catalysis, which accomplishes the site-selective functionalization of an electronically unbiased C–H bond[18]. Varying the enzyme cavity by mutation of amino-acid residues at the active pockets of toluene monooxygenase leads to modular and regiospecific oxidation[19]. The intriguing correlation between the configurational structure of the enzyme and site-selectivity incentivized the work of Davies et al. showing enantioselective differentiation of the pervasive non-activated sp^3 C–H bonds without directing groups, but via subtly modified spatial arrangement of chiral dirhodium catalysts[20–22]. The catalyst-controlled strategy was also efficiently used to selectively functionalize the *para*-C–H bond by the introduction of a sterically hindered co-catalyst or ligand[23–27] (Fig. 1b). However, these systems are tied to metal catalysis, and asymmetric variants remain under-represented.

Over the last three decades, organocatalysis[28,29] has emerged as a powerful catalysis platform that is gradually being incorporated into the routine synthetic toolbox to obtain chiral molecules[30–34]. However, organocatalytic site- and enantioselective functionalization of inactive aryl C–H bonds remains in its infancy, largely due to the scarcity of organocatalysts with activating potency that compares favourably to metal catalysts, as well as the high energy barrier encountered during the dearomatization process. The capability of finely tuned organocatalysts carrying an enzyme-like chiral microenvironment to foster stereoinduction in challenging asymmetric reactions, as well as the tunability of the chiral control region[35–40], prompted our postulation of an organocatalytic reaction mode to realize long-range enantiocontrolled functionalization of the *para*-C–H bond of arene. Our previous findings[41] showed that interaction between a chiral phosphoric acid (CPA)[42–45] and an azo group directs activation towards the adjacent carbon centre on the naphthalene ring under mild conditions. By analogy to enzymatic catalysis[19], where the site-selectivity of a reaction is modulated by the spatial position of residues at the active site, we envisioned achieving asymmetric functionalization of arene *para*-C–H bonds by methodical modulation of the activation channel in the CPA catalyst, as well as tactical introduction of the azo functionality on substrates as an association point (Fig. 1c). Contrary to classic electrophilic aromatic substitution (S_EAr) reactions[4], this nucleophilic aromatic substitution (S_NAr) protocol enables a fundamental shift to utilize nucleophilic reactants, thus broadening the substrate choices and avoiding the latent side reactions that otherwise beleaguer S_EAr reactions because of the substituent orientation effect. Concurrently, a nucleophilic addition onto a single benzene ring exerts more drastic aromaticity disruption compared to the naphthalene system, and thus necessitates a more ideal reactivity

[1]Shenzhen Grubbs Institute and Department of Chemistry, Guangdong Provincial Key Laboratory of Catalysis, Southern University of Science and Technology, Shenzhen, China. [2]College of Materials, Chemistry and Chemical Engineering, Hangzhou Normal University, Hangzhou, China. [3]Academy for Advanced Interdisciplinary Studies, Southern University of Science and Technology, Shenzhen, China. [4]These authors contributed equally: Jian-Hui Mao, Yong-Bin Wang, Limin Yang. ✉e-mail: wangyb@sustech.edu.cn; tanb@sustech.edu.cn

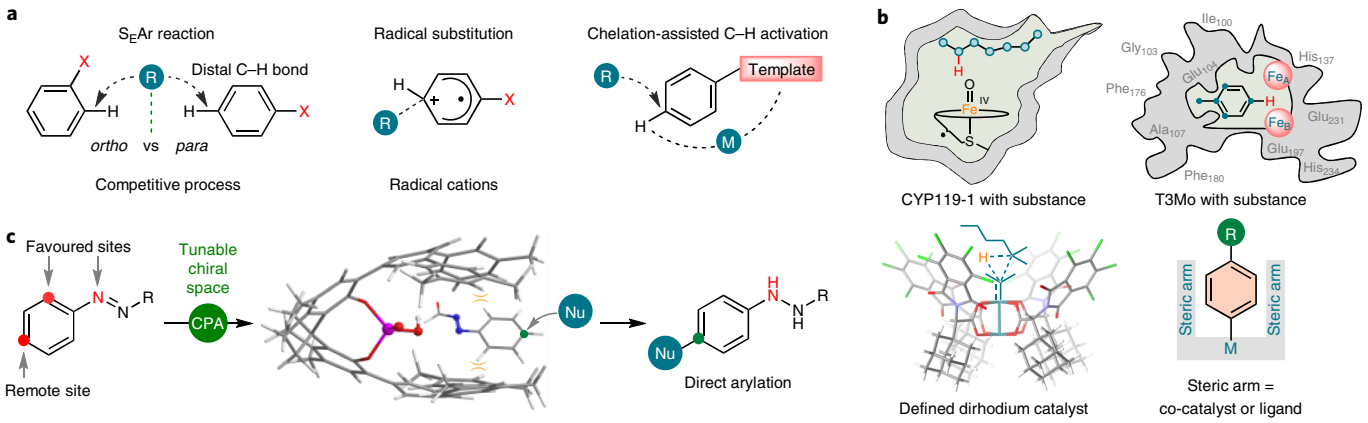

Fig. 1 | Selective functionalization of C–H bonds and our design blueprint. a, Substituent-directed *para*-selective C–H functionalization, including classic electrophilic aromatic substitution (S_EAr) reactions, radical substitution and a chelation-assisted C–H activation strategy. **b**, Catalyst-controlled site-selective C–H functionalization in enzyme and metal catalysis. Enzymes adjust the site-selectivity of C–H activation reactions by changing the spatial configuration of the active pocket. Metal catalysis can also achieve site-selective C–H activation by adjusting the spatial structure of the ligands. **c**, Organocatalyst-controlled *para*-selective and enantioselective arene C–H functionalization. High site-selective and enantioselective arene C–H functionalization is achieved through organocatalysed nucleophilic aromatic substitution (S_NAr) of azobenzenes.

channel to counterbalance the high activation energy via an enhanced substrate–catalyst interaction. We further posited projecting substituents onto the CPA backbone to hinder the approach of reactants and suppress *C*-functionalization of the *ortho*-carbon and *N*-functionalization at the azo entity, making available the *para*-C–H bond for activation. Judicious selection of other reacting partners that can facilely approach and form effectual binding with the active site of CPA is equally instrumental. Ultimately, precise enantiocontrol at the distant *para* position calls for extraordinarily effective chiral recognition of substrates by the CPA catalyst. Guided by these propositions, we have realized a robust organocatalytic system to give exquisite control of site- and stereoselectivity in *para*-C–H bond functionalization of azobenzene compounds with diversified *C*-nucleophiles.

Results and discussion

Reaction development. Because a confined reactivity pocket may be inaccessible for sterically demanding nucleophiles, and small nucleophilic reactants could endanger selectivity control, we chose elaborated oxazolone nucleophiles possessing synthetic potential as cyclic precursors of amino acids to verify our hypothesis. As shown in Fig. 2a, the initial trial began by treating azobenzene **1a** with oxazolone **2a** and a catalytic amount of achiral Brønsted acid **C1** in CH_2Cl_2 at room temperature. The 12-h reaction yielded a product mixture composed of the *ortho*-C–H functionalization product (**3a-C-*ortho***) as the major component and azo-functionalization adduct **3a-N** in 16% yield, without any targeted **3a-C-*para*** (Fig. 2a, entry 1). This was in line with a dominating *ortho*-C–H bond activation when the steric shielding impact from the catalyst is not there to obstruct the native reaction sites. We next surveyed a collection of CPAs bearing varied axially chiral backbones and began to observe trace formation of **3a-C-*para*** (6% yield, 50% e.e.) when **C4** with a 3,5-dimethylphenyl group at both the 3- and 3′-positions of the 1,1′-bi-2,2′-naphthol (BINOL) scaffold was used (Fig. 2a, entry 4). In line with our hypothesis, product distributions with respect to site selection were found to be dependent on the steric bulk of the core backbones in the CPAs surveyed (Fig. 2a, entries 2–11), as displayed in the bar chart in Fig. 2b. When a 1,1′-spirobiindane-7,7′-diol (SPINOL)-derived **C10** was included, **3a-C-*para*** was the major product, with 66% yield and extraordinary enantiopurity (Fig. 2a, entry 10). Subsequent examination revealed a superiority of acetonitrile over other tested solvents. Performing the titled transformation at higher reaction molarity and with prolonged duration finally afforded **3a-C-*para*** in 92% yield (optimal conditions; Fig. 2a, entry 15). Notably, outstanding enantioinduction was consistently imposed by most CPAs bearing sufficiently bulky substituents, regardless of the other reaction parameters. This substantiated the decisive role of the unique interactions between CPA and the oxazolone nucleophile in this catalysis protocol.

Substrate scope. With establishment of the optimal reaction conditions, we set out to evaluate the substrate generality of azobenzene derivative **1**, as outlined in Table 1. Absolute enantiocontrol was similarly observed for azobenzene with an ethyl ester group (in place of the methyl ester) to provide *para*-selective product **3b** in 84% yield. Installing *ortho*-substituents relative to the azo handle, such as methyl, methoxy and methylthio groups and halides, had a negligible influence on the reaction outcomes, regardless of electronic property (**3c–3h**). Other isomers of disubstituted azobenzenes with *meta* substitution gave chiral molecules **3j–3l** in relatively lower yields, except the methyl congener (**3i**). Interestingly, extremely high efficiency was restored with the addition of a C2 substituent (**3m–3o**). The moderate yields obtained for 3,5-disubstitued azo substrates could indicate the presence of an undesired steric effect during nucleophilic addition (**3q** and **3r**). A subsequent probe of the oxazolones scope afforded an array of highly enantioenriched amino-acid precursors (**3s–3ae**) in yields ranging from 69 to 98% and e.e. values exceeding 99%, demonstrating the compatibility of oxazolone substrates with the current catalytic system. Other than the benzyl-type substituents, cyclohexyl and isopropyl groups containing oxazolones were also well suited, with the beneficial effect of C2 substitution in this transformation evident. Subsequently, oxindole **4a**, a similar prochiral *C*-nucleophile, was treated under standard conditions with the chosen substrate, 2-methoxy-substituted azobenzene **1d**. The high yield of *para*-selective adduct **5a** (95%) and virtually vanishing enantioinduction (2% e.e.) when using the same catalyst **C10** suggested a sustained CPA–azo group association bypassing reactions on the nitrogen and *ortho*-carbon centres, but a reduced enantio-discrimination due to the specificity of the chiral cavity. As shown in Table 2, changing to **C12**, embracing the same SPINOL scaffold, notably enhanced the enantioselectivity to 95% in CCl_4, without erosion of efficiency. Oxindoles **4** with a broad range

a

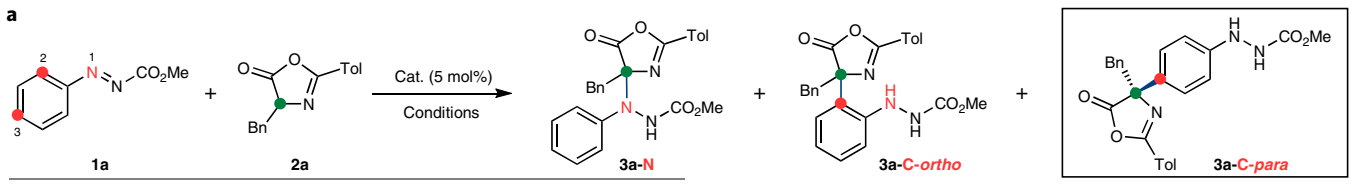

Entry[a]	Cat.	Solvent	Isolated yield (%) 3a-N	3a-C-*ortho*[c]	3a-C-*para*	e.e. (%)[b] 3a-C-*para*
1	**C1**	CH_2Cl_2	16	49	0	–
2	(*rac*)-**C2**	CH_2Cl_2	27	64	0	–
3	(*R*)-**C3**	CH_2Cl_2	15	54	Trace	67
4	(*R*)-**C4**	CH_2Cl_2	15	36	6	50
5	(*R*)-**C5**	CH_2Cl_2	13	19	7	92
6	(*R*)-**C6**	CH_2Cl_2	19	9	3	>99
7	(*R*)-**C7**	CH_2Cl_2	13	24	2	91
8	(*S*)-**C8**	CH_2Cl_2	19	22	11	99
9	(*S*)-**C9**	CH_2Cl_2	8	12	19	>99
10	(*S*)-**C10**	CH_2Cl_2	7	8	66	>99
11	(*R*)-**C11**	CH_2Cl_2	15	4	54	–99
12	(*S*)-**C10**	$CHCl_3$	35	4	33	>99
13	(*S*)-**C10**	DCE	7	9	51	>99
14	(*S*)-**C10**	CH_3CN	5	5	78	>99
15[d]	(*S*)-**C10**	CH_3CN	Trace	Trace	92	>99

b

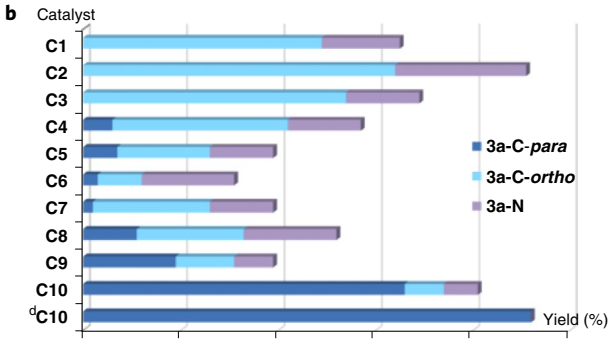

c

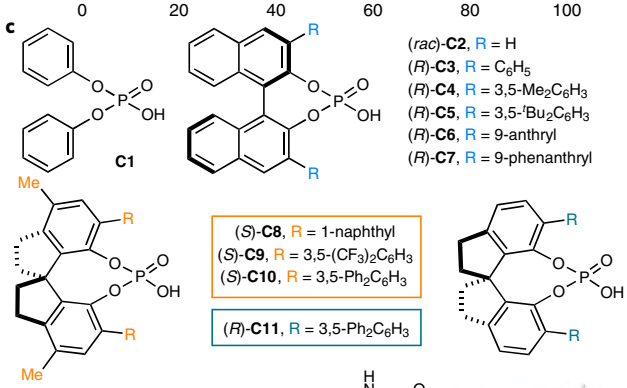

d

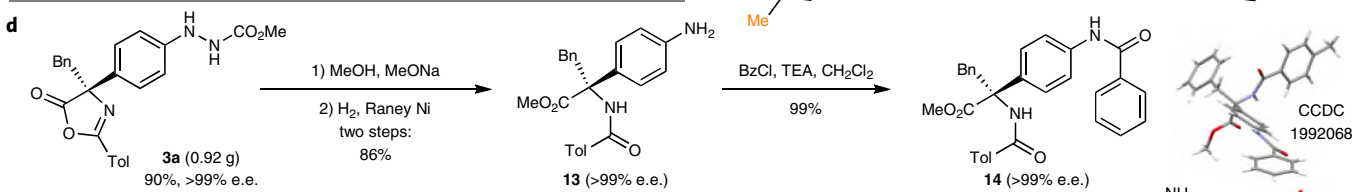

e

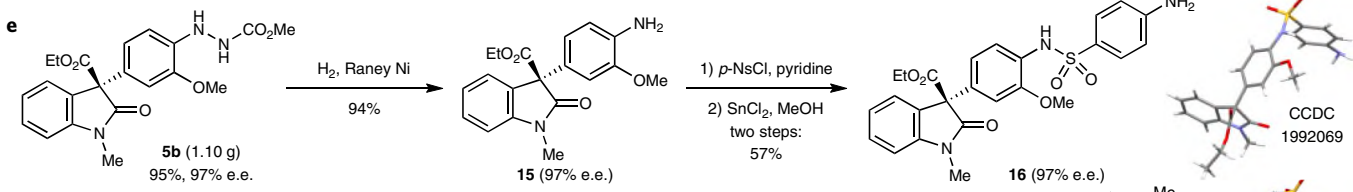

f

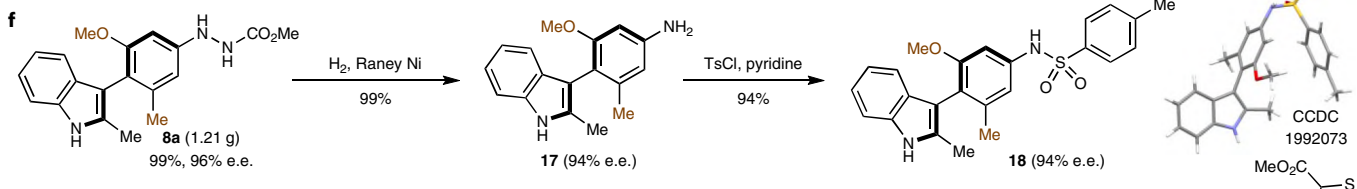

g

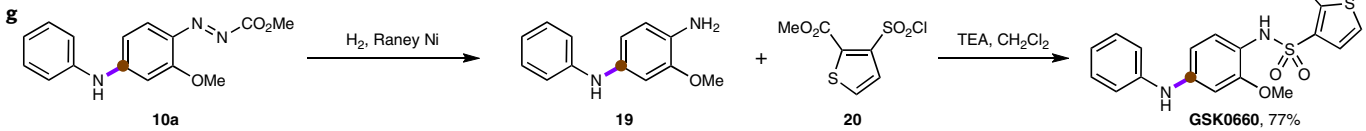

Fig. 2 | Condition optimization and transformations. a, Summary of the reaction outcomes for all generated products and selectivities. [a]Reaction carried out with **1a** (0.10 mmol), **2a** (0.12 mmol) and catalyst (5 mol%) in 2.0 ml of solvent at r.t. for 12 h, unless noted otherwise. [b]The e.e. values were determined by HPLC analysis using a chiral stationary phase. [c]Contains other compounds derived from **3a-C-*ortho***. [d]0.5 ml of CH_3CN was used and the reaction proceeded for 36 h. **b**, Site selectivity for the examined CPAs. **c**, CPA structures. **d**, Transformation of **3a** to amino-acid derivatives. The absolute configuration of **3a** was derived from the X-ray diffraction analysis of **14**. **e**, Derivatization of compound **5b**. The absolute configuration of **5b** was derived from the X-ray diffraction analysis of **16**. **f**, Derivatization of compound **8a**. The absolute configuration of **8a** was derived from the X-ray diffraction analysis of **18**. **g**, Two-step synthesis of bioactive **GSK0660** from amination products **10a**.

Table 1 | Organocatalysed arene C–H functionalization with oxazolones under condition A

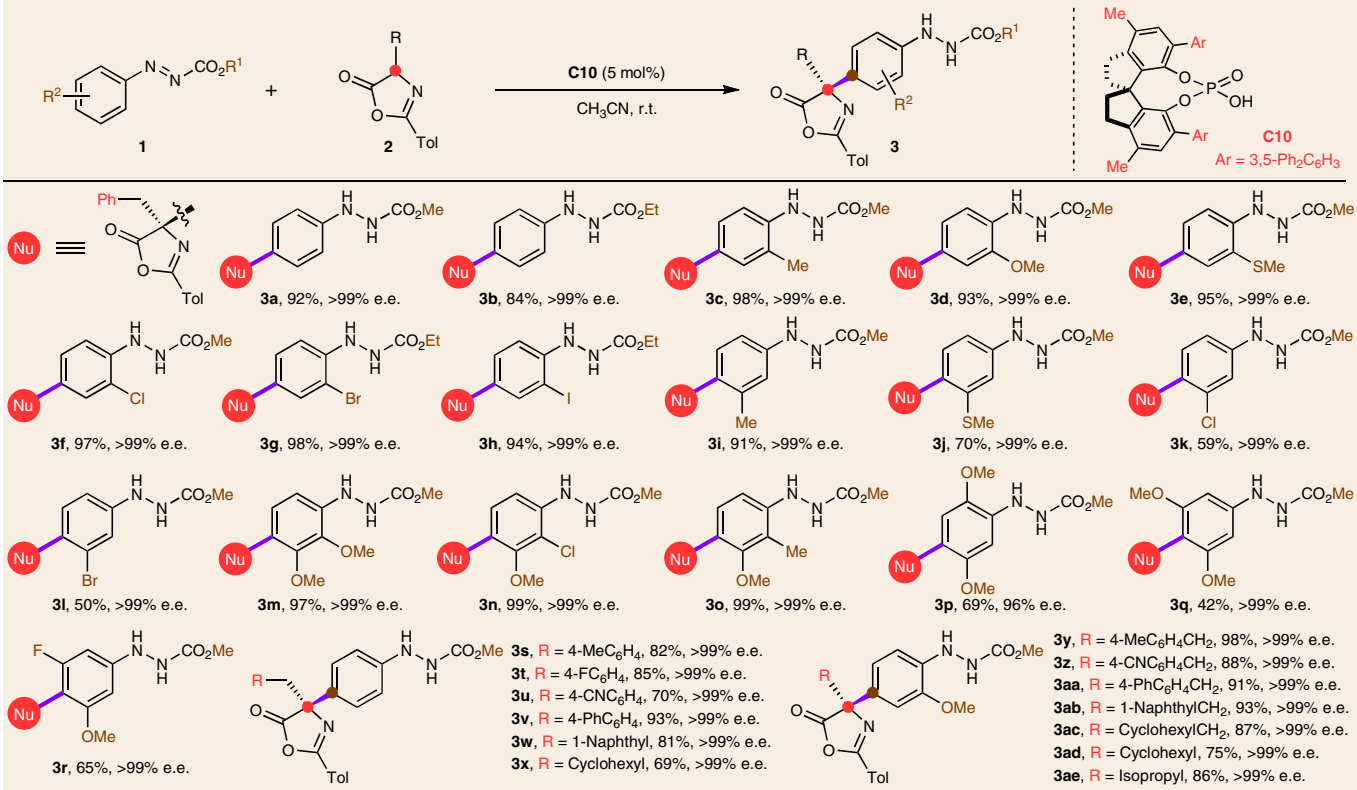

Condition A: all reactions were carried out with **1** (0.10 mmol), **2** (0.12 mmol), **C10** (5 mol%) and CH_3CN (0.5 ml) at room temperature for 36 h. The e.e. values were determined using HPLC analysis.

Table 2 | Organocatalysed arene C–H functionalization with oxindoles under condition B

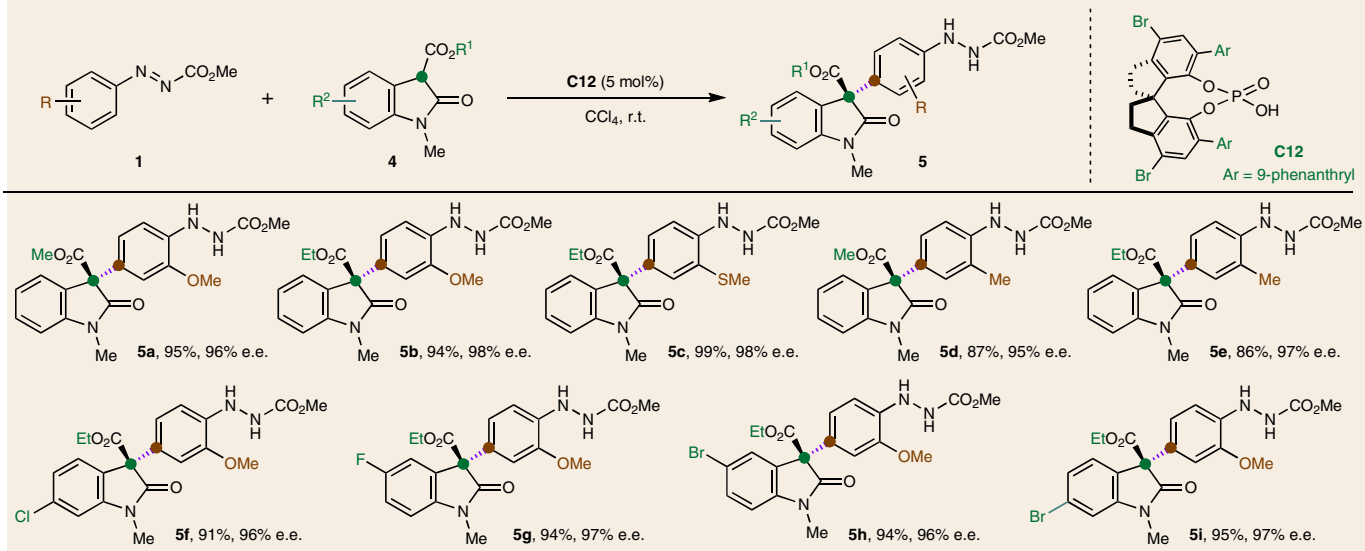

Condition B: all reactions were carried out with **1** (0.10 mmol), **4** (0.12 mmol), **C12** (5 mol%) and CCl_4 (2.0 ml) at room temperature for 12–36 h. The e.e. values were determined using HPLC analysis.

of substituents and substituent patterns were tested to give the corresponding products **5** carrying a quaternary carbon stereocentre, in excellent yields and enantioselectivities (**5a–5i**).

The established strategy for asymmetric access to two classes of quaternary carbon stereocentres with excellent *para*- and enantioselectivities stimulated our exploration of aromatic *C*-nucleophiles to synthesize biaryl structures. Indole derivatives **6** of comparable size to the substantiated nucleophiles were first considered. Experimental results for the reaction between indole **6a** and azobenzene **1a** with respect to representative CPAs are summarized in Supplementary Table S2. Similarly, achiral **C1** and (*rac*)-**C2** without 3,3′-substituents on the BINOL skeleton delivered a trace amount of the desired *para*-addition heterobiaryl **7a** in this system on account of competitive addition onto the azo group. Similar results were

Table 3 | Organocatalysed arene C–H functionalization with indoles under conditions C and D

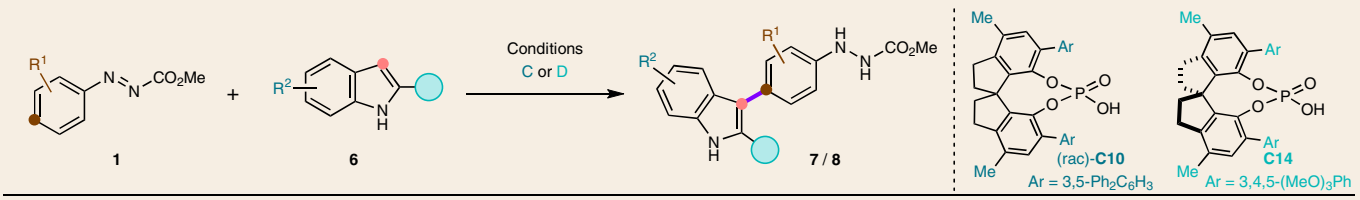

Achiral products: Condition C

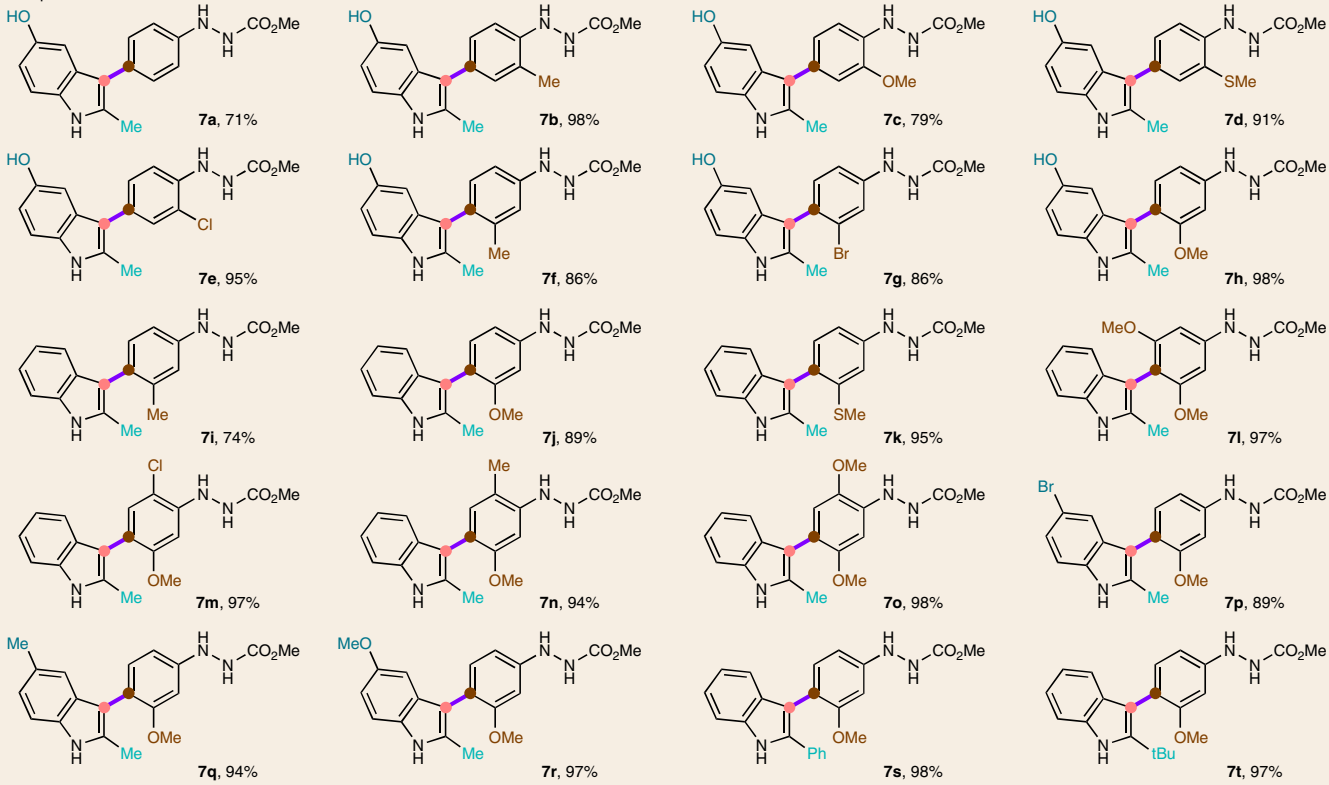

Axially chiral products: Condition D

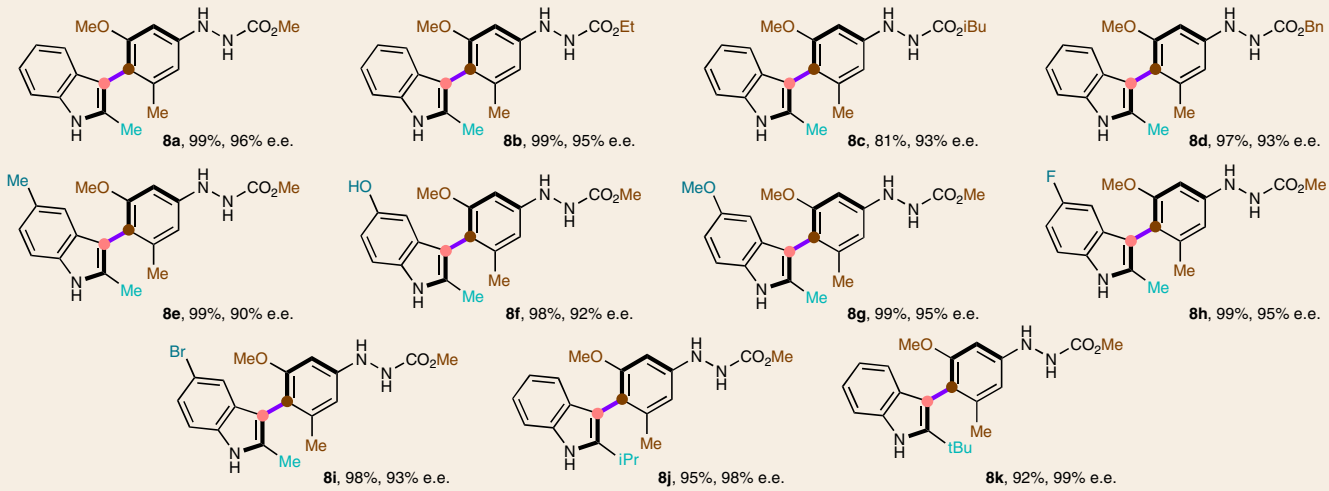

Condition C: all reactions were carried out with **1** (0.20 mmol), **6** (0.24 mmol), (*rac*)-**C10** (5 mol%) and CH_2Cl_2 (2.0 ml) at room temperature for 0.5–120 h. Condition D: all reactions were carried out with **1** (0.20 mmol), **6** (0.24 mmol), **C14** (2 mol%) and CH_2Cl_2 (2.0 ml) at −40 °C for 6–120 h. The e.e. values were determined using HPLC analysis.

obtained for **C7** and **C8**, which could not provide a suitable cavity to position the substrates in a favourable fashion. Pleasingly, both racemic and enantiopure **C10**, with verified and well-organized spatial configuration, boosted the *para*-selective functionalization efficiency to 71% yield in 24 h, whereas **C13**, which provided a stronger π–π interaction with the reactant, gave rise to lower efficiency (for details see Supplementary Table 2). Unfruitful investigations of other reaction parameters to improve the reaction outcome further demonstrated the unique correlation between site-selectivity and the three-dimensional structure of the catalyst.

Table 4 | Arene *para*-activation using anilines under condition E

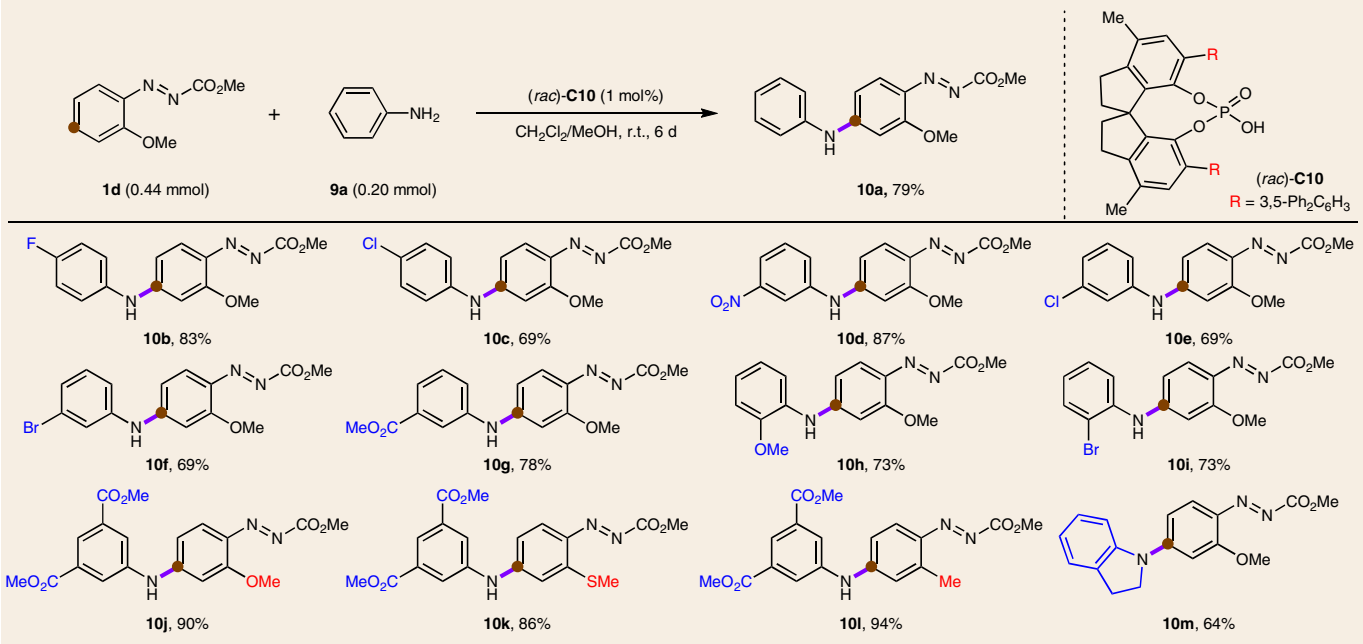

Condition E: all reactions were carried out with **1** (0.20–0.44 mmol), **9** (0.10–0.20 mmol), (*rac*)-**C10** (1–5 mol%) and MeOH/CH_2Cl_2 (0.25–2.0 ml) at room temperature for 24–240 h. The e.e. values were determined using HPLC analysis.

The generality of the indole-aryl structures was exploited by the current *para*-selective C–H functionalization strategy. As shown in Table 3, a wide range of azobenzenes **1** were surveyed, and noticeably improved transformation yields were demonstrated on substrates bearing one or two substituents on the aromatic ring (**7b–7t**). This reaction was also amendable to halogen-atom-containing substrates and formed the desired heterobiaryls with remarkable efficiencies (**7e** and **7g**). The installation of a strong electron-donating group at the *meta* position of azobenzene exhibited a commendable positive effect reflected in high product yields (**7j–7o**). Negative results were obtained when using the indoles without substituents at the 2-position as substrates (for details see Supplementary Fig. 6), indicating that the 2-substituents play a critical role in the transformation. It should be noted that substitution patterns on 2-substituted indoles exerted a negligible influence on the reaction outcomes (**7p–7t**). Moreover, the excellent yield of product **7l** with di-*meta*-substituted azobenzene suggested the implementation of an atroposelective variant with the current protocol.

Accordingly, the assembly of enantioenriched aryl-indole atropisomers was launched by exposing 3,5-disubstituted azobenzene **1v** to 2-methylindole **6b** under the developed standard conditions. The targeted atropisomer **8a** was produced in near quantitative yield (97%) but modest atroposelectivity (52% e.e.) with (*S*)-**C10**, while (*rac*)-**C10** forged racemic **8a** in a similar excellent yield. Subtle modification of the SPINOL framework in the CPA structure presented **C14** as the optimal facilitator. As shown in Table 3, a range of azobenzenes and indoles were investigated for this atroposelective transformation to deliver the respective axially chiral adducts with outstanding enantiocontrol (**8a–8k**). In particular, this reaction exhibited good tolerance to the electron-withdrawing ester moiety on azobenzene partners, axial rotation restriction groups, as well as the C5 substituent on indole substrates.

The attested capability of CPA in activating the *para* position of azobenzene offered opportunities to expand on the diversity of nucleophiles. Beyond *C*-nucleophiles, aniline **9a** could be engaged as the *N*-nucleophile to realize *N*-arylation (Table 4). With catalyst (*rac*)-**C10**, the desirable C–N bond was forged between aniline **9a** and azobenzene **6c** with impressive site-selectivity (**10a**). Notably, the conventionally formed hydrazine was unstable in this transformation due to its low oxidation potential and spontaneously converted to azo by the oxidation of azobenzene[41,46]. Thus, excess azobenzene was added to completely oxidize the hydrazine for this class of substrates to simplify the reaction system. In contrast to other tested nucleophiles, a longer reaction duration was essential for better conversion due to the potential catalyst deactivation induced by basic anilines (Table 4). Electron-poor ester groups on the 3,5-positions of aniline could allay this adverse effect, giving satisfactory reaction efficiencies (**10j–10l**). Indoline, representing a secondary amine substrate, was incorporated in **10m** in a synthetically useful yield. This arene C–H amination protocol provided to be an effective complementary method to conventional transition-metal catalytic variants, which often proceed under harsh conditions. Subsequently, 2-mercaptopyridine **11a** was chosen and verified as a competent *S*-nucleophile to assemble diaryl thioether **12a** in commendable yield and selectivity (*para*/others > 20/1) with catalyst (*rac*)-**C10** in CH_2Cl_2 or acetonitrile (Table 5). It should be pointed out that on switching the catalyst to **C1**, the reaction efficiency for **12a** was compromised pronouncedly as a result of the dominant formation of by-products. With **11a** as a model nucleophile, a wide array of azobenzenes worked well for this reaction to generate aryl-thiolated compounds **12b–12q** in moderate to excellent yields (Table 5). In contrast to the earlier reactions, halide substituent(s) on azobenzene could hamper the product yield and site-selectivity (**12d–12e**, **12h–12i** and **12p–12q**). Meanwhile, 2-mercaptobenzoxazole (**11b**), 2-mercaptobenzothiazole (**11c** and **11d**) as well as 1,3,4-thiadiazole-2-thiol (**11e**) complied well with this chemistry to provide **12n–12w** in high *para* selectivities and yields. Additionally, control experiments (Supplementary Fig. 7) revealed that the sp^2-N in the *S*-nucleophiles plays a critical role in the control of *para* selectivity and reactivity.

Transformation of chiral products. To test the scalability and practicality of the developed protocol, a gram-scale synthesis of compound **3a** was implemented with the standard set of conditions.

Table 5 | Arene *para*-activation using arylthiols under condition F

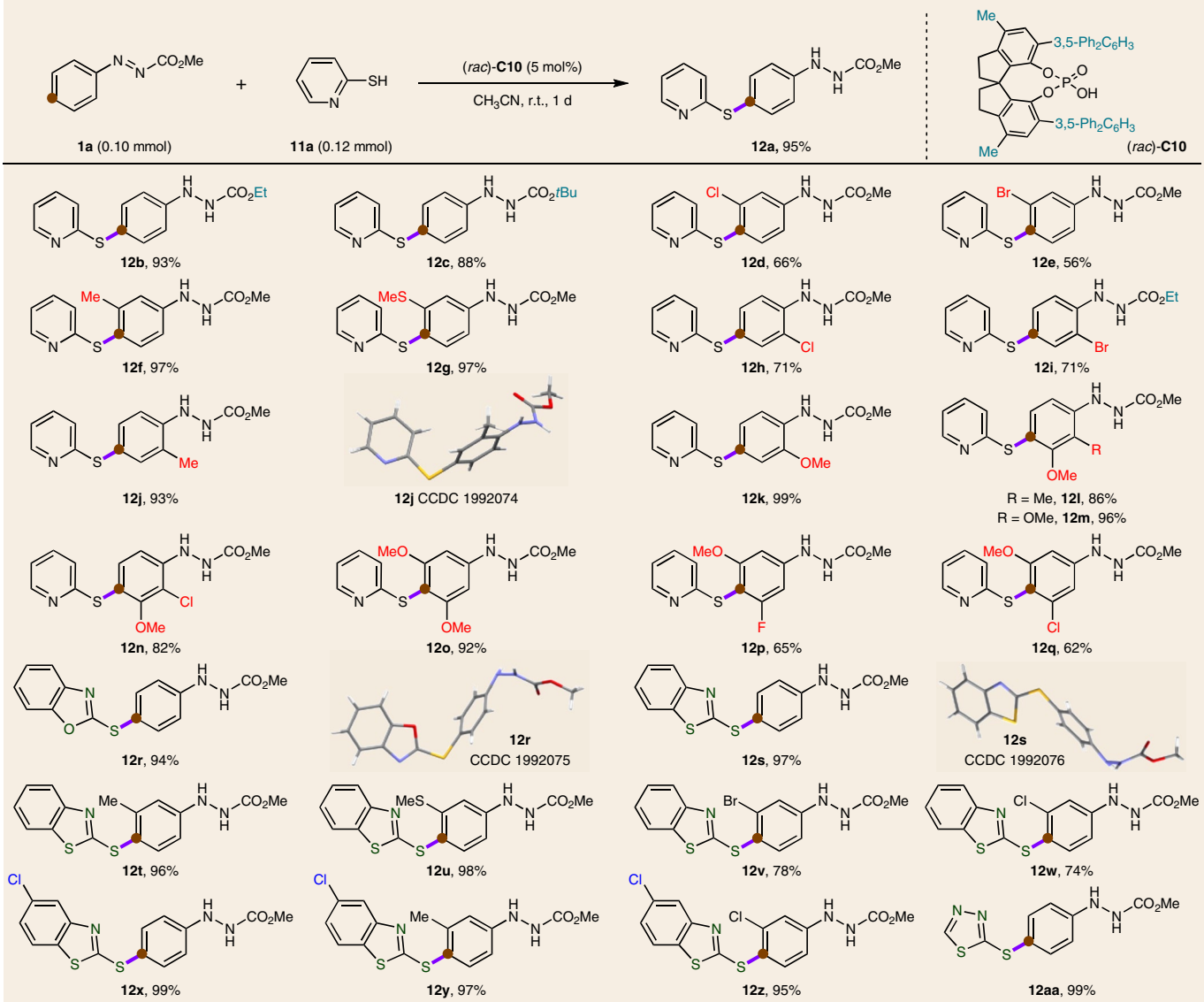

Condition F: all reactions were carried out with **1** (0.10 mmol), **11** (0.12–0.14 mmol), (*rac*)-**C10** (5 mol%) and CH_3CN (0.50–2.0 ml) at room temperature for 12–96 h. The e.e. values were determined using HPLC analysis.

As displayed in Fig. 2d, the synthesis efficiency and enantiocontrol observed for the small-scale reaction were perfectly preserved. The ring-opening reaction of adduct **3a** with sodium methoxide and subsequent hydrogenation with Raney nickel gave the chiral amino-acid derivative **13** in 86% yield, without any loss of stereochemical integrity. Facile benzoylation of **13** generated compound **14** in near quantitative yield, for which the absolute configuration was determined by X-ray diffraction analysis (CCDC 1992068) as *R* and the configurations of other products were assigned by analogy. Similarly, 1.1 g of **5b** was assembled from **1d** and **4b** in excellent yield and enantiopurity. Cleavage of the N–N bond by Raney nickel under H_2 atmosphere gave the free amine-containing structure **15** in 94% yield. The absolute configuration of the sulfonylated congener **16** was established by X-ray diffraction analysis (CCDC 1992069) as *R*; compounds **5** as well as precursor **15** were designated analogously (Fig. 2e). Conserved reactivity and selectivity were correspondingly achieved in scaled-up atroposelective formation of axially chiral compounds, as exemplified by heterobiaryl **8a**. Hydrogenation of **8a** reliably gave product **17** in quantitative yield (loss of 2% e.e.). Tosylation then gave compound **18**, and the absolute configuration for this class of atropisomerically enriched products (CCDC 1992073) was determined by X-ray diffraction analysis of the representative derivative **18** (Fig. 2f). Finally, a bioactive molecule **GSK0660** was synthesized from the amination product **10a** in two steps with 77% overall yield, further illustrating the utility of this strategy (Fig. 2g).

Mechanistic studies. Kinetic studies showed a distinct linear relationship between the initial reaction rates and catalyst concentrations, hinting that the reaction was first order with respect to the catalyst (Fig. 3b,c). These results, combined with the linear relationship between the enantiopurities of the product and the catalyst, indicated that only one CPA molecule participates in the rate- and enantio-determining step[47,48]. To provide experimental evidence, we designed and synthesized deuterium-labelled azobenzene **1a-*d*1** and **1a-*d*5** for isotopic labelling studies. We also investigated the products and reaction rates of the *para*-selective C–H functionalization of **1a**, **1a-*d*1** and **1a-*d*5** separately. Under

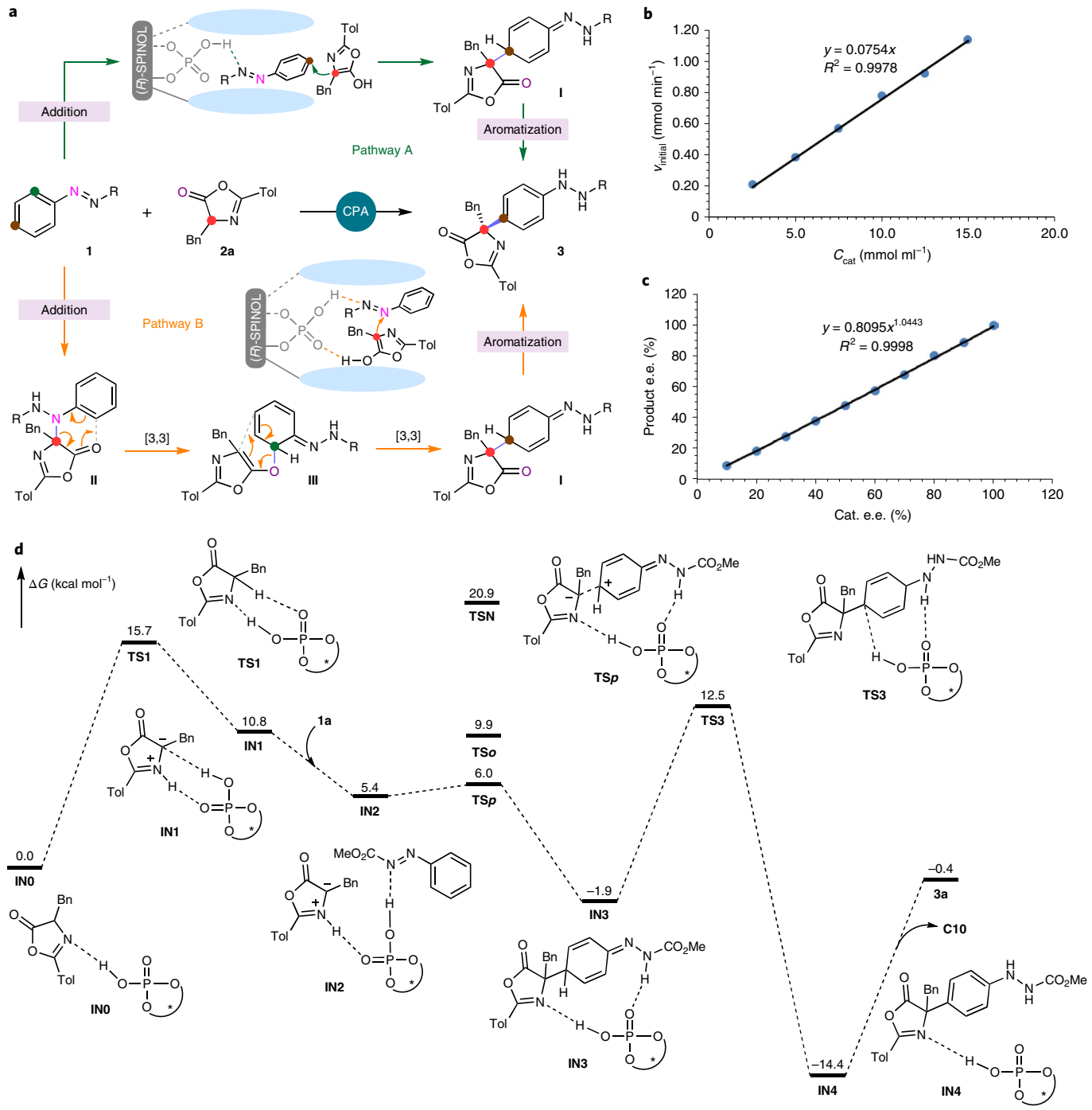

Fig. 3 | Proposed reaction pathways and mechanistic studies. a, Pathway A: direct nucleophilic addition on the *para* site of azobenzene. Pathway B: nucleophilic addition on the azo group, followed by two-fold [3,3]-sigmatropic rearrangement. **b**, Kinetic study, showing that the transformation for **3a** shows a distinct linear relationship between the initial reaction rate ($v_{initial}$) and catalyst concentration (C_{cat}). Corresponding data can be found on pages 6–8 of the Supplementary Information. **c**, Graph of the enantiopurity correlation between product and catalyst, showing a linear relationship. Corresponding data can be found on page 8 of the Supplementary Information. **d**, Calculated free-energy profile for the formation of **3a**. Energies are given in kcal mol^{-1}. ΔG, Gibbs free energy change; TS, transition state.

standard conditions, **1a**-*d***1** smoothly afforded product **3a** in 93% yield and >99% e.e., while **3a**-*d***4** was generated from **1a**-*d***5** in 90% yield and >99% e.e. Kinetic analysis of these labelling experiments showed that the kinetic isotope effect of **1a**/**1a**-*d***1** was 1.07 and that of **1a**/**1a**-*d***5** was 0.907, indicating that C–H bond cleavage is not the rate-determining step of the catalytic cycle (for details, see pages 8 and 9 in the Supplementary Information). However, these experimental results were not able to definitively determine the transition states and reaction mechanism of the *para*-selective arene C–H functionalization. A mechanistic delineation of the aforementioned transformations was put forward as depicted in Fig. 3a, guided by experimental observations. The control experiments showed that products **3a**-**N** could not be converted to desired product **3a**-C-***para*** under standard conditions. These observations

ruled out pathway B[49,50], which commences from nucleophilic addition on the azo group, followed by two-fold [3,3]-sigmatropic rearrangement[51]. To investigate the origins of site selectivities during C–H functionalization, density functional theory calculations were conducted on the reaction between **1a** and **2a** with **C10** as catalyst. In the calculated free-energy profile for the reaction (Fig. 3d), the CPA **C10** and oxazolone **2a** form a relatively stable reactant complex **IN0**, with the imine entity acting as proton acceptor in the hydrogen bonding with the catalyst. With the CPA operating as a bifunctional catalyst and proton shuttle, the reaction is initiated by the deprotonation of oxazolone **2a** to form münchnone-type intermediate **IN1**. An additional hydrogen bond formed between azobenzene **1a** and the bifunctional Brønsted acid catalyst results in a relatively stable intermediate **IN2**. An ensuing nucleophilic attack of the deprotonated oxazolone on different positions of the activated azo arene species will lead to regioisomeric products, including **3a-C-*para***, **3a-C-*ortho*** and **3a-N**. The transition state **TSp** for *re*-face addition of the deprotonated oxazolone to the *para* carbon of the phenyl ring on the activated azo arene species is energetically most favoured, with a reaction barrier of only 6.0 kcal mol^{-1}, and thus leads to the major product **3a-C-*para*** (for details, see pages 13 and 14 in the Supplementary Information).

Conclusion

Although organocatalysis has emerged as a powerful chemical tool for various synthetic transformations, application to direct arene activation has not been trivial, especially when chemo-, site- and enantioselectivities are also primary considerations. We have showcased a highly efficient arene activation tactic in which diversified nucleophiles can be engaged to afford a wide range of *para*-selective functionalization products. This chemistry capitalizes on the successful merger of CPA and azobenzene derivatives, in which the CPA facilitates hydrogen-bond-associated catalytic generation of an active intermediate, where the association could supplement the CPA to mediate arene activation. At the same time, the well-organized chiral cavity of CPA enables enantio-discrimination when control of central or axial chirality is viable. The optical purities of all chiral products were maintained with high fidelity on conversion to the respective derivatives and, notably, enantiopure amino-acid derivatives could be synthesized facilely. It is expected that this distinctive use of CPA catalysis to coordinate the reactivity of active species for controllable aromatic ring activation may be of broad interest to practitioners pursuing selective elaboration of arenes and constitutes a practical alternative to existing strategies.

Online content

Any methods, additional references, Nature Research reporting summaries, source data, extended data, supplementary information, acknowledgements, peer review information; details of author contributions and competing interests; and statements of data and code availability are available at https://doi.org/10.1038/s41557-021-00750-x.

Received: 21 September 2020; Accepted: 8 June 2021;
Published online: 09 August 2021

References

1. Abrams, D. J., Provencher, P. A. & Sorensen, E. J. Recent applications of C–H functionalization in complex natural product synthesis. *Chem. Soc. Rev.* **47**, 8925–8967 (2018).
2. Wencel-Delord, J. & Glorius, F. C–H bond activation enables the rapid construction and late-stage diversification of functional molecules. *Nat. Chem.* **5**, 369–375 (2013).
3. Yamaguchi, J., Yamaguchi, A. D. & Itami, K. C–H bond functionalization: emerging synthetic tools for natural products and pharmaceuticals. *Angew. Chem. Int. Ed.* **51**, 8960–9009 (2012).
4. Zhou, Z. & Parr, R. G. Activation hardness: new index for describing the orientation of electrophilic aromatic substitution. *J. Am. Chem. Soc.* **112**, 5720–5724 (1990).
5. Dey, A., Maity, S. & Maiti, D. Reaching the south: metal-catalyzed transformation of the aromatic *para*-position. *Chem. Commun.* **52**, 12398–12414 (2016).
6. Romero, N. A., Margrey, K. A., Tay, N. E. & Nicewicz, D. A. Site-selective arene C–H amination via photoredox catalysis. *Science* **349**, 1326–1330 (2015).
7. Boursalian, G. B., Ham, W. S., Mazzotti, A. R. & Ritter, T. Charge-transfer-directed radical substitution enables *para*-selective C–H functionalization. *Nat. Chem.* **8**, 810–815 (2016).
8. Berger, F. et al. Site-selective and versatile aromatic C–H functionalization by thianthrenation. *Nature* **567**, 223–228 (2019).
9. Bag, S. et al. Remote *para*-C–H functionalization of arenes by a D-shaped biphenyl template-based assembly. *J. Am. Chem. Soc.* **137**, 11888–11891 (2015).
10. Maji, A. et al. Experimental and computational exploration of *para*-selective silylation with a hydrogen-bonded template. *Angew. Chem. Int. Ed.* **56**, 14903–14907 (2017).
11. Patra, T. et al. Palladium-catalyzed directed *para* C–H functionalization of phenols. *Angew. Chem. Int. Ed.* **55**, 7751–7755 (2016).
12. Hoque, M. E., Bisht, R., Haldar, C. & Chattopadhyay, B. Noncovalent interactions in Ir-catalyzed C–H activation: L-shaped ligand for *para*-selective borylation of aromatic esters. *J. Am. Chem. Soc.* **139**, 7745–7748 (2017).
13. Maji, A. et al. H-bonded reusable template assisted *para*-selective ketonisation using soft electrophilic vinyl ethers. *Nat. Commun.* **9**, 3582 (2018).
14. Dey, A., Sinha, S. K., Achar, T. K. & Maiti, D. Accessing remote *meta*- and *para*-C(sp^2)–H bonds with covalently attached directing groups. *Angew. Chem. Int. Ed.* **58**, 10820–10843 (2019).
15. Dutta, U. et al. Rhodium catalyzed template-assisted distal *para*-C–H olefination. *Chem. Sci.* **10**, 7426–7432 (2019).
16. Pimparkar, S. et al. *Para*-selective cyanation of arenes by H-bonded template. *Chem. Eur. J.* **26**, 11558–11564 (2020).
17. Shi, H. et al. Differentiation and functionalization of remote C–H bonds in adjacent positions. *Nat. Chem.* **12**, 399–404 (2020).
18. Rittle, J. & Green, M. T. Cytochrome P450 compound I: capture, characterization and C–H bond activation kinetics. *Science* **330**, 933–937 (2010).
19. Fishman, A., Tao, Y., Rui, L. & Wood, T. K. Controlling the regiospecific oxidation of aromatics via active site engineering of toluene *para*-monooxygenase of *Ralstonia pickettii* PKO1. *J. Biol. Chem.* **280**, 506–514 (2005).
20. Liao, K., Negretti, S., Musaev, D. G., Bacsa, J. & Davies, H. M. L. Site-selective and stereoselective functionalization of unactivated C–H bonds. *Nature* **533**, 230–234 (2016).
21. Liao, K. et al. Site-selective and stereoselective functionalization of non-activated tertiary C–H bonds. *Nature* **551**, 609–613 (2017).
22. Liao, K. et al. Design of catalysts for site-selective and enantioselective functionalization of non-activated primary C–H bonds. *Nat. Chem.* **10**, 1048–1055 (2018).
23. Cheng, C. & Hartwig, J. F. Rhodium-catalyzed intermolecular C–H silylation of arenes with high steric regiocontrol. *Science* **343**, 853–857 (2014).
24. Ma, B. et al. Highly para-selective C–H alkylation of benzene derivatives with 2,2,2-trifluoroethyl α-aryl-α-diazoesters. *Angew. Chem. Int. Ed.* **56**, 2749–2753 (2017).
25. Okumura, S. et al. *para*-Selective alkylation of benzamides and aromatic ketones by cooperative nickel/aluminum catalysis. *J. Am. Chem. Soc.* **138**, 14699–14704 (2016).
26. Saito, Y., Segawa, Y. & Itami, K. *para*-C–H borylation of benzene derivatives by a bulky iridium catalyst. *J. Am. Chem. Soc.* **137**, 5193–5198 (2015).
27. Yang, L., Semba, K. & Nakao, Y. *para*-Selective C–H borylation of (hetero) arenes by cooperative iridium/aluminum catalysis. *Angew. Chem. Int. Ed.* **56**, 4853–4857 (2017).
28. List, B., Lerner, R. A. & Barbas, C. F. III Proline-catalyzed direct asymmetric aldol reactions. *J. Am. Chem. Soc.* **122**, 2395–2396 (2000).
29. Ahrendt, K. A., Borths, C. J. & MacMillan, D. W. C. New strategies for organic synthesis: the first highly enantioselective organocatalytic Diels–Alder reaction. *J. Am. Chem. Soc.* **122**, 4243–4244 (2000).
30. Taylor, M. S. & Jacobsen, E. N. Asymmetric catalysis by chiral hydrogen-bond donors. *Angew. Chem. Int. Ed.* **45**, 1520–1543 (2006).
31. Mukherjee, S., Yang, J. W., Hoffmann, S. & List, B. Asymmetric enamine catalysis. *Chem. Rev.* **107**, 5471–5569 (2007).
32. MacMillan, D. W. C. The advent and development of organocatalysis. *Nature* **455**, 304–308 (2008).
33. Silvi, M. & Melchiorre, P. Enhancing the potential of enantioselective organocatalysis with light. *Nature* **554**, 41–49 (2018).

34. Metrano, A. J. & Miller, S. J. Peptide-based catalysts reach the outer sphere through remote desymmetrization and atroposelectivity. *Acc. Chem. Res.* **52**, 199–215 (2019).
35. Chen, J. et al. Carbonyl catalysis enables a biomimetic asymmetric Mannich reaction. *Science* **360**, 1438–1442 (2018).
36. Tsuji, N. et al. Activation of olefins via asymmetric Brønsted acid catalysis. *Science* **359**, 1501–1505 (2018).
37. Pupo, G. et al. Asymmetric nucleophilic fluorination under hydrogen bonding phase-transfer catalysis. *Science* **360**, 638–642 (2018).
38. Gustafson, J. L., Lim, D. & Miller, S. J. Dynamic kinetic resolution of biaryl atropisomers via peptide-catalyzed asymmetric bromination. *Science* **328**, 1251–1255 (2010).
39. Lin, S. & Jacobsen, E. N. Thiourea-catalysed ring opening of episulfonium ions with indole derivatives by means of stabilizing non-covalent interactions. *Nat. Chem.* **4**, 817–824 (2012).
40. Knowles, R. R. & Jacobsen, E. N. Attractive noncovalent interactions in asymmetric catalysis: links between enzymes and small molecule catalysts. *Proc. Natl Acad. Sci. USA* **107**, 20678–20685 (2010).
41. Jung, D., Jang, S. H., Yim, T. & Kim, J. Oxidation potential tunable organic molecules and their catalytic application to aerobic dehydrogenation of tetrahydroquinolines. *Org. Lett.* **20**, 6436–6439 (2018).
42. Akiyama, T., Itoh, J., Yokota, K. & Fuchibe, K. Enantioselective Mannich-type reaction catalyzed by a chiral Brønsted acid. *Angew. Chem. Int. Ed.* **43**, 1566–1568 (2004).
43. Uraguchi, D. & Terada, M. Chiral Brønsted acid-catalyzed direct Mannich reactions via electrophilic activation. *J. Am. Chem. Soc.* **126**, 5356–5357 (2004).
44. Akiyama, T. Stronger Brønsted acids. *Chem. Rev.* **107**, 5744–5758 (2007).
45. Parmar, D., Sugiono, E., Raja, S. & Rueping, M. Complete field guide to asymmetric BINOL-phosphate derived Brønsted acid and metal catalysis: history and classification by mode of activation; Brønsted acidity, hydrogen bonding, ion pairing and metal phosphates. *Chem. Rev.* **114**, 9047–9153 (2014).
46. Hansch, C., Leo, A. & Taft, R. W. A survey of Hammett substituent constants and resonance and field parameters. *Chem. Rev.* **91**, 165–195 (1991).
47. Chen, M. & Sun, J. Catalytic asymmetric *N*-alkylation of indoles and carbazoles through 1,6-conjugate addition of aza-*para*-quinone methides. *Angew. Chem. Int. Ed.* **56**, 4583–4587 (2017).
48. Ma, D., Miao, C.-B. & Sun, J. Catalytic enantioselective House–Meinwald rearrangement: efficient construction of all-carbon quaternary stereocenters. *J. Am. Chem. Soc.* **141**, 13783–13787 (2019).
49. Uyeda, C. & Jacobsen, E. N. Transition state charge stabilization through multiple non-covalent interactions in the guanidinium-catalyzed enantioselective Claisen rearrangement. *J. Am. Chem. Soc.* **133**, 5062–5075 (2011).
50. Li, G.-Q. et al. Organocatalytic aryl–aryl bond formation: an atroposelective [3,3]-rearrangement approach to BINAM derivatives. *J. Am. Chem. Soc.* **135**, 7414–7417 (2013).
51. Qi, L.-W., Mao, J.-H., Zhang, J. & Tan, B. Organocatalytic asymmetric arylation of indoles enabled by azo groups. *Nat. Chem.* **10**, 58–64 (2017).

Methods

Method A. To a solution of **2** (0.12 mmol) and **C10** (4.0 mg, 0.005 mmol) in CH_3CN (0.5 ml), **1** (0.10 mmol) was added. After stirring for 36 h at room temperature, the mixture was directly purified by flash column chromatography on silica gel (eluted with PE/DCM/EtOAc) to give enantiopure product **3**.

Method B. To a solution of oxindole **4** (0.12 mmol) and **C12** (3.4 mg, 0.005 mmol) in CCl_4 (2.0 ml), **1** (0.10 mmol) was added. After stirring for 12 h at room temperature, the mixture was directly purified by flash column chromatography on silica gel (eluted with PE/DCM/EtOAc) to give pure product **5**.

Method C. To a solution of **1** (0.2 mmol), (*rac*)-**C10** (8.0 mg, 0.010 mmol) in DCM (2.0 ml), indole **6** (0.24 mmol) was added at room temperature. The reaction was stirred until compound **1** was completely consumed (detected by thin layer chromatography). If a side product from the oxidization of product was detected, Hantzsch ester (0.10 mmol) should be added into the reaction and stirred for another 6 h. The resulting solution was directly purified by flash column chromatography on silica gel (eluted with PE/EtOAc) to give pure product **7**.

Data availability

The X-ray crystallographic coordinates for the products reported in this Article have been deposited at the Cambridge Crystallographic Data Centre (CCDC), under deposition nos. CCDC 1992074 (**12j**), CCDC 1992075 (**12r**), CCDC 1992076 (**12s**), CCDC 1992068 (**14**), 1992069 (**16**) and 1992073 (**18**). Copies of the data can be obtained free of charge via https://www.ccdc.cam.ac.uk/structures/. Experimental procedures and characterization of new compounds are available in the Supplementary Information.

Acknowledgements

We are grateful for financial support from the National Natural Science Foundation of China (grants 21825105 to B.T. and 21801121 to Y.-B.W.), Guangdong Provincial Key Laboratory of Catalysis (grant 2020B121201002 to B.T.), Guangdong Innovative Program (grant 2019BT02Y335 to B.T.), Shenzhen Special Funds (grants JCYJ20180305123508258 to S.-H.X. and JCYJ20180302174106405 to Y.-B.W.), Shenzhen Nobel Prize Scientists Laboratory Project and SUSTech Special Fund for the Construction of High-Level Universities (grant G02216402, B.T.). We dedicate this paper to the 100th Anniversary of Xiamen University.

Author contributions

B.T. conceived and directed the project. J.-H.M. and Y.-B.W. designed and performed experiments. L.Y. performed the density functional theory calculations and mechanism analysis. S.-H.X., S.L., Q.-H.W., Y.C., Q.L. and J.L. helped with the collection of some new compounds and data analysis. B.T., S.-H.X., Y.-B.W., S.L. and L.Y. wrote the manuscript with input from all other authors. All authors discussed the results and commented on the manuscript.

Competing interests

The authors declare no competing interests.

Additional information

Supplementary information The online version contains supplementary material available at https://doi.org/10.1038/s41557-021-00750-x.

Correspondence and requests for materials should be addressed to Y.-B.W. or B.T.

Peer review information *Nature Chemistry* thanks Debabrata Maiti and the other, anonymous, reviewer(s) for their contribution to the peer review of this work.

Reprints and permissions information is available at www.nature.com/reprints.